

Least-Squares Finite Element Methods for nonlinear problems: A unified framework

Fleurianne Bertrand^a, Maximilian Brodbeck^b, Tim Ricken^b, Henrik Schneider^c

^aTechnische Universität Chemnitz, Fakultät für Mathematik, Reichenhainer Straße 41, Chemnitz, 09126, Sachsen, Germany

^bUniversität Stuttgart, Institut für Statik und Dynamik der Luft- und Raumfahrtkonstruktionen, Pfaffenwaldring 27, Stuttgart, 70569, Baden-Württemberg, Germany

^cUniversität Duisburg-Essen, Fakultät für Mathematik, Thea-Leymann-Straße 9, Essen, 45127, Nordrhein-Westfalen, Germany

Abstract

This paper presents a unified Least-Squares framework for solving nonlinear partial differential equations by recasting the governing system as a residual minimization problem. A Least-Squares functional is formulated and the corresponding Gauss–Newton iterative method derived, which approximates simultaneously primal and stress-like variables. We derive conditions under which the Least-Squares functional is coercive and continuous in an appropriate solution space, and establish convergence results while demonstrating that the functional serves as a reliable a posteriori error estimator. This inherent error estimation property is then exploited to drive adaptive mesh refinement across a variety of problems, including the stationary heat equation with either temperature-dependent or discontinuous conductivity or a ReLU-type nonlinearity, nonlinear elasticity based on the Saint Venant–Kirchhoff model and sea-ice dynamics.

Keywords: Least-Squares Finite Element Method, nonlinear partial differential equations, a posteriori error estimator, adaptive mesh refinement

1. Introduction

Nonlinear partial differential equations (PDEs) are ubiquitous in modeling complex physical phenomena across science and engineering. Owing to their rigorous theoretical foundation, versatility, computational efficiency, and ability to handle irregular domains, Finite Element Methods (FEM) have proven to be an indispensable tool for approximating PDE solutions. Within many of these finite element approaches, a primal variable u minimizes an energy potential over a bounded domain Ω with Lipschitz boundary in $H^1(\Omega) = \{v \in L^2(\Omega) : \|\nabla v\|_{L^2(\Omega)} < \infty\}$. However, these purely primal approaches often suffer from reduced robustness and fail to provide accurate approximations of certain physically relevant quantities. To circumvent this so-called locking phenomena, mixed finite element methods introduce a dual quantity σ to be approximated in $H(\text{div}, \Omega) = \{\sigma \in L^2(\Omega)^2 : \|\text{div } \sigma\|_{L^2(\Omega)} < \infty\}$. A major challenge of these methods are the required inf-sup conditions, both at the continuous and discrete levels, to ensure well-posedness and stability. These conditions impose constraints on the choice of finite element spaces, requiring careful pairing of function spaces for primal- and dual variables. Failure to satisfy the inf-sup condition can lead to unstable or inaccurate solutions, making the selection of appropriate finite element spaces a nontrivial task, see [2].

Least-Squares Finite Element Methods (LSFEM) (see e.g. [4]) provide an attractive alternative to classical mixed finite element methods by minimizing specifically designed Least-Squares functionals. Unlike mixed methods, LSFEM eliminates the need for inf-sup compatible function spaces and avoids the complexities associated with saddle point formulations. Another key advantage is the built-in a posteriori error estimate, which can directly be utilized in adaptive refinement strategies. LSFEM has been successfully applied to a wide range of linear partial differential equations, including the Poisson problem [14], linear elasticity [6, 18] or flow problems [5].

Since the resulting system of linear equations is inherently symmetric and positive definite, LSFEM allows the use of efficient linear equation solvers, making it particularly well-suited for nonlinear problems. Gauss-Newton and multilevel methods, as developed in [17], enable the extension of LSFEM to nonlinear problems, which is crucial in applications such as nonlinear elasticity [9, 12, 16] or general flow problems [17, 13]. Despite these advantages, a

systematic analysis of LSFEM in the nonlinear setting remains largely absent in literature. In particular, while the Least-Squares functional in the linear case inherently provides an a posteriori error estimate, there has been limited exploration of how this property can be extended the nonlinear case. The purpose of this paper is to bridge this gap by developing a general framework that extends this property to broader classes of problems.

In the following, section 2 introduces the Least-Squares framework for nonlinear PDEs, formulating the residual-based functional and deriving the corresponding Gauss-Newton iterative scheme. Section 3 provides a detailed analysis of the theoretical properties of the Least-Squares functional, establishing conditions for coercivity, continuity, and convergence. In particular, we prove that the Least-Squares functional serves as a reliable a posteriori error estimator in the nonlinear setting, thereby extending its well-known properties from the linear case. Section 4 applies the developed framework to various nonlinear PDEs, including a stationary heat equation with temperature-dependent conductivity, nonlinear elasticity using the Saint Venant–Kirchhoff model, and a model for sea-ice dynamics. Additionally, we discuss extensions to problems with discontinuous coefficients and ReLU-type nonlinearities.

2. The Least-Squares approach

Let Ω be an open, bounded Lipschitz domain of \mathbb{R}^d with $d \in \{2, 3\}$. Given a Hilbert Space \mathbf{V} , the nonlinear system of first-order partial differential equations under consideration reads

$$\mathcal{R}(\mathbf{u}) + \mathbf{f} = \mathbf{0} \quad (1)$$

for $\mathbf{u} \in \mathbf{V}$. Throughout this work, the existence of a solution $\mathbf{u}^* \in \mathbf{V}$ is assumed and the nonlinear functional $\mathcal{F}(\mathbf{u}) = \|\mathcal{R}(\mathbf{u}) + \mathbf{f}\|_{\mathbf{H}}^2$ is minimized in a suitable Hilbert Space \mathbf{H} . The corresponding Fréchet derivative \mathcal{R}' of the operator \mathcal{R} is given by

$$\lim_{\|\mathbf{h}\|_{\mathbf{V}} \rightarrow 0} \frac{1}{\|\mathbf{h}\|_{\mathbf{V}}} \|\mathcal{R}(\mathbf{u} + \mathbf{h}) - \mathcal{R}(\mathbf{u}) - \mathcal{R}'(\mathbf{u}) \mathbf{h}\|_{\mathbf{H}}, \quad (2)$$

allowing the computations of gradient and hessian of the functional \mathcal{F} :

$$\begin{aligned} \nabla \mathcal{F}(\mathbf{u}) &= (\mathcal{R}'(\mathbf{u}))^* (\mathcal{R}(\mathbf{u}) + \mathbf{f}), \\ \nabla^2 \mathcal{F}(\mathbf{u}) &= (\mathcal{R}'(\mathbf{u}))^* \mathcal{R}'(\mathbf{u}) + (\mathcal{R}''(\mathbf{u}))^* (\mathcal{R}(\mathbf{u}) + \mathbf{f}). \end{aligned}$$

Using these quantities, the classical Newton method for minimizing \mathcal{F} is expressed as

$$\mathbf{u}_{n+1} = \mathbf{u}_n - \left(\nabla^2 \mathcal{F}(\mathbf{u}_n) \right)^{-1} \nabla \mathcal{F}(\mathbf{u}_n).$$

To avoid its potentially expensive evaluation, $\mathcal{R}''(\mathbf{u}_0)$ can be neglected if \mathbf{u}_0 is close to the solution \mathbf{u}^* . This leads to the Gauss-Newton method, defined by the iterative process

$$\mathbf{u}_{n+1} = \mathbf{u}_n - \mathcal{R}'(\mathbf{u}_n)^{-1} (\mathbf{f} + \mathcal{R}(\mathbf{u}_n)), \quad (3)$$

i.e.

$$\mathbf{u}_{n+1} = \mathbf{u}_n + \delta \mathbf{u} \quad \text{with} \quad \mathcal{R}'(\mathbf{u}_n) \delta \mathbf{u} = -\mathbf{f} - \mathcal{R}(\mathbf{u}_n). \quad (4)$$

Note that the Gauss-Newton method is equivalent to the Newton method for the residual \mathcal{R} , since $\mathcal{R}(\mathbf{u}^*) = 0$. To fully exploit the advantages of the Least-Squares method, in particular its inherent error estimator property, the Newton step is reformulated as the minimization of a linear Least-Squares functional

$$\mathcal{F}_{\text{lin}}(\mathbf{v}; (\mathbf{u}_n, \mathbf{f})) := \|\mathcal{R}'(\mathbf{u}_n) \mathbf{v} + \mathbf{f} + \mathcal{R}(\mathbf{u}_n)\|_{\mathbf{H}}^2,$$

to obtain

$$\delta \mathbf{u} = \arg \min_{\mathbf{v} \in \mathbf{V}} \mathcal{F}_{\text{lin}}(\mathbf{v}; (\mathbf{u}_n, \mathbf{f})). \quad (5)$$

The Lax-Milgram Lemma implies the equivalence of the Least-Squares functional and the norm $\|\cdot\|_{\mathbf{V}}$

$$C_e \|\mathbf{w}\|_{\mathbf{V}} \leq \|\mathcal{R}'(\mathbf{u}_n) \mathbf{w}\|_{\mathbf{H}} \leq C_c \|\mathbf{w}\|_{\mathbf{V}} \text{ for all } \mathbf{w} \in \mathbf{V}, \quad (6)$$

is a sufficient condition for the well-posedness of the Gauss-Newton step (4). In particular, the minimization problem (5) has a unique minimizer. This result guarantees the practicability of the Gauss-Newton method outlined in Algorithm 1.

Algorithm 1 Generic Gauss-Newton algorithm

Require: initial guess \mathbf{u}_0

Set $n := 0$

while stopping criterion not met **do**

 Determine the Newton direction by solving

$$\delta \mathbf{u}_n = \arg \min_{\mathbf{v} \in \mathbf{V}} \mathcal{F}_{\text{lin}}(\mathbf{v}; (\mathbf{u}_n, \mathbf{f}))$$

 Set $\mathbf{u}_{n+1} = \mathbf{u}_n + \delta \mathbf{u}_n$

 Set $n = n + 1$

end while

Since the Gauss-Newton method is equivalent to a Newton method for the residual operator \mathcal{R} , the established convergence theory for Newton methods (see [19, 7]) is directly applicable. The following general result, establishing the conditions under which the Newton method is well-defined and guarantees superlinear or quadratic convergence, is recalled.

Theorem 2.1. *Suppose $\mathcal{R} : \mathbf{V} \rightarrow \mathbf{H}$ and $\mathbf{f} \in \mathbf{H}$ and let \mathbf{u}^* be a solution of $\mathcal{R}(\mathbf{u}) = \mathbf{0}$. Moreover, let the Fréchet derivative of $\mathcal{R}(\mathbf{u})$ exists for all \mathbf{u} in an open neighborhood of \mathbf{u}^* and (6) holds for $\mathbf{u}_n = \mathbf{u}^*$. Then, there exists $\varepsilon > 0$ such that it holds:*

- (a) *For any initial guess \mathbf{u}_0 in $B(\mathbf{u}^*, \varepsilon)$, the Newton method is well-defined and generates a sequence (\mathbf{u}_n) which converges superlinearly to \mathbf{u}^* .*
- (b) *\mathbf{u}^* is the unique solution of (1) in $B(\mathbf{u}^*, \varepsilon)$.*
- (c) *If additionally \mathcal{R}' is Hölder continuous with exponent γ and constant L in $B(\mathbf{u}^*, \varepsilon)$, then the convergence rate increase to $1 + \gamma$. In particular, if \mathcal{R}' is Lipschitz continuous $B(\mathbf{u}^*, \varepsilon)$, then the method converges quadratically.*

In order to minimize a linearized functional, the solution $\delta \mathbf{u} \in \mathbf{V}$ has to fulfill

$$(\mathcal{R}'(\mathbf{u}_n) [\delta \mathbf{u}], \mathcal{R}'(\mathbf{u}_n) [\mathbf{v}]) = (-\mathbf{f} - \mathcal{R}(\mathbf{u}_n), \mathcal{R}'(\mathbf{u}_n) [\mathbf{v}]) \quad (7)$$

for all $\mathbf{v} \in \mathbf{V}$. The energy balance (6) implies the well-posedness of the minimization of the Least-Squares functional in any finite dimensional subspace $\mathbf{V}_{\mathcal{T}}$ based on a triangulation \mathcal{T} of Ω . Up to a constant, the error of the finite element solution is bounded by the best approximation error

$$\begin{aligned} \|\mathbf{u}_{n+1} - \mathbf{u}_{n+1, \mathcal{T}}\|_{\mathbf{V}} &= \|\mathbf{u}_n + \delta \mathbf{u} - \mathbf{u}_n - \delta \mathbf{u}_{\mathcal{T}}\|_{\mathbf{V}} = \|\delta \mathbf{u} - \delta \mathbf{u}_{\mathcal{T}}\|_{\mathbf{V}} \\ &\leq \frac{1}{C_e} \left\| -\mathbf{f} - \mathcal{R}(\mathbf{u}_n) - \mathcal{R}'(\mathbf{u}_n) (\delta \mathbf{u}_{\mathcal{T}}) \right\| = \frac{1}{C_e} \mathcal{F}_{\text{lin}}(\delta \mathbf{u}_{\mathcal{T}}) \\ &= \frac{1}{C_e} \min_{\mathbf{v} \in \mathbf{V}_{\mathcal{T}}} \mathcal{F}_{\text{lin}}(\mathbf{v}) = \frac{1}{C_e} \min_{\mathbf{v} \in \mathbf{V}_{\mathcal{T}}} \mathcal{F}_{\text{lin}}(\mathbf{v} - \delta \mathbf{u}) \leq \frac{C_c}{C_e} \min_{\mathbf{v} \in \mathbf{V}_{\mathcal{T}}} \|\mathbf{v} - \delta \mathbf{u}\|. \end{aligned} \quad (8)$$

This leads to the inexact Newton method, outlined in Algorithm 2.

Algorithm 2 Inexact Gauss-Newton algorithm

Require: initial guess \mathbf{u}_0

Set $n := 0$

while stopping criterion not met **do**

 Determine the Newton direction by solving

$$\delta \mathbf{u}_{n,\mathcal{T}} = \arg \min_{\delta \mathbf{u} \in \mathbf{V}_{\mathcal{T}}} \|\mathcal{R}'(\mathbf{u}_n) \delta \mathbf{u} - \mathbf{f} + \mathcal{R}(\mathbf{u}_n)\|_{\mathbf{H}}^2$$

 Set $\mathbf{u}_{n+1,\mathcal{T}} = \mathbf{u}_{n,\mathcal{T}} + \delta \mathbf{u}_{n,\mathcal{T}}$

 Set $n = n + 1$

end while

The following convergence theorem holds under the additional assumption of a sufficiently good approximation of the Newton step, realized by a forcing sequence.

Theorem 2.2. *Let the assumptions of theorem 2.1 hold and a forcing sequence $\{\eta_n\}$ exist with $0 < \eta_n < 1$ such that*

$$\mathcal{F}_{\text{lin}}(\delta \mathbf{u}_n; (\mathbf{u}_n; \mathbf{f})) \leq \eta_n \mathcal{F}(\mathbf{u}_{n+1}) \text{ for } n = 0, 1, \dots \quad (9)$$

Then, there exists $\varepsilon > 0$ such that it holds:

- (a) *For any initial guess \mathbf{u}_0 in $B(\mathbf{u}^*, \varepsilon)$, the inexact Newton method is well-defined and generates a sequence (\mathbf{u}_n) which converges to \mathbf{u}^* .*
- (b) *The sequence (\mathbf{u}_n) generated by Algorithm 2, converges superlinearly.*
- (c) *If additionally \mathcal{R}' is Lipschitz continuous on $B(\mathbf{u}^*, \varepsilon)$, then (\mathbf{u}_n) generated by Algorithm 2 converges quadratically.*

Based on the results discussed above, the Least-Squares approach, combined with the Gauss-Newton method, offers a computationally efficient and theoretically robust framework for addressing nonlinear systems of PDEs. Subsequent sections build on these foundational results by refining the assumptions to align with the typical structure of nonlinear PDEs encountered in practical applications.

3. A unified framework

The theoretical and computational framework presented so far, relies on general assumptions about the residual operator \mathcal{R} and its Fréchet derivative. However, in many practical applications, the underlying PDE system exhibits additional structure and constraints that can be exploited to refine the convergence analysis. This section introduces new assumptions designed to leverage these structural properties. In many practical applications, the system $\mathcal{R}(\mathbf{u}) + \mathbf{f} = \mathbf{0}$ often consists of multiple coupled equations. These equations typically involve the primal variable u and additional flux or stress variables σ , introduced in Section 1. One of the equations then represents the a conservation law, such as the conservation of momentum. It is usually linear in u and σ and reads

$$L_1(u, \sigma) + f = 0$$

with a linear function $L_1(u, \sigma)$. The second equation, commonly representing the constitutive equation, frequently exhibits a nonlinearity in u and reads

$$L_2(u, \sigma) + K(u) + g = 0$$

with a linear function $L_2(u, \sigma)$ and a nonlinear function $K(u)$. This can be cast into the system

$$\mathcal{R}(\mathbf{u}) = \mathbf{f} \quad \text{with} \quad \mathcal{R}(\mathbf{u}) = \begin{pmatrix} L_1(u, \sigma) \\ L_2(u, \sigma) + K(u) \end{pmatrix} \quad \text{and} \quad \mathbf{f} = \begin{pmatrix} f \\ g \end{pmatrix}.$$

The resulting Least-Squares functional reads

$$\mathcal{F}(u, \sigma; f, g) = \|L_1(u, \sigma) + f\|_H^2 + \|L_2(u, \sigma) + K(u) + g\|_H^2. \quad (10)$$

Recall that the norm equivalence (6) substantiates the convergence analysis of the Newton method. Consequently, the first assumption imposes an energy balance assumption on the linear part, i.e. the coercivity and continuity properties in the linear case.

Assumption 1. *There exists positive constants C_1, \dots, C_6 such that the following norm-equivalence holds*

$$C_1\|u\|_U^2 + C_2\|\sigma\|_\Sigma^2 \leq \|L_1(u, \sigma)\|_H^2 + \|L_2(u, \sigma)\|_H^2 \quad (11a)$$

$$\|L_1(u, \sigma)\|_H^2 \leq C_3\|u\|_U^2 + C_4\|\sigma\|_\Sigma^2 \quad (11b)$$

$$\|L_2(u, \sigma)\|_H^2 \leq C_5\|u\|_U^2 + C_6\|\sigma\|_\Sigma^2 \quad (11c)$$

for all $u, \sigma \in U \times \Sigma$.

Next, to control the nonlinear component of the PDE system, a Lipschitz continuity condition is imposed on the nonlinear term $K(u)$, restricting its growth and ensuring boundedness within a suitable set.

Assumption 2. *There exists an open and non-empty set $S \subset U$ such that*

$$\|K(u) - K(v)\|_H^2 \leq L\|u - v\|_U^2 \quad (12)$$

holds for all $u, v \in S$ with a Lipschitz constant $0 < L < C_1$.

With the assumptions on the linear and nonlinear components in place, a crucial norm equivalence result for the linearized Least-Squares functional \mathcal{F}_{lin} can now be established. This equivalence guarantees the existence and uniqueness of solutions to the associated minimization problem and forms the basis for analyzing convergence. The following theorem formalizes this result.

Theorem 3.1. *Let Assumptions 1 and 2 hold true. For any $u \in S$ with $K(u)$ Fréchet differentiable in u , the norm-equivalence*

$$\|v\|_U^2 + \|\tau\|_\Sigma^2 \lesssim \|L_1(v, \tau)\|_H^2 + \|L_2(v, \tau) + K'(u)v\|_H^2 \lesssim \|v\|_U^2 + \|\tau\|_\Sigma^2 \quad (13)$$

holds true for all $(v, \tau) \in U \times \Sigma$. In particular, the Least-Squares problem (5) has a unique solution.

Proof. Since $K(u)$ is Fréchet differentiable, the Fréchet derivative can be bounded by the Lipschitz constant, i.e. it holds $\|K'(u)\|^2 \leq L$. The triangle inequality, together with (11), implies

$$\begin{aligned} \|L_1(v, \tau)\|_H^2 + \|L_2(v, \tau) + K'(u)v\|_H^2 &\leq \|L_1(v, \tau)\|_H^2 + 2\|L_2(v, \tau)\|_H^2 + 2\|K'(u)v\|_H^2 \\ &\leq (C_3 + 2C_5)\|v\|_U^2 + (C_4 + 2C_6)\|\tau\|_\Sigma^2 + 2\|K'(u)\|^2\|v\|_U^2 \\ &\leq (C_3 + 2C_5 + 2L)\|v\|_U^2 + (C_4 + 2C_6)\|\tau\|_\Sigma^2. \end{aligned}$$

On the other hand, equation (11) implies

$$\begin{aligned} \|L_1(v, \tau)\|^2 + \|L_2(v, \tau) + K'(u)v\|^2 &\geq \|L_1(v, \tau)\|^2 + \|L_2(v, \tau)\|^2 - \|K'(u)v\|^2 \\ &\geq C_1\|v\|_U^2 + C_2\|\tau\|_\Sigma^2 - \|K'(u)\|^2\|v\|_U^2, \end{aligned}$$

such that the crucial assumption $C_1 - L > 0$ concludes the proof with

$$\|L_1(v, \tau)\|^2 + \|L_2(v, \tau) + K'(u)v\|^2 \geq (C_1 - L)\|v\|_U^2 + C_2\|\tau\|_\Sigma^2.$$

□

Algorithm 3 AFEM-loop

loopDetermine $\delta \mathbf{u}_n$ by (inexactly) solving

$$\delta \mathbf{u}_n = \arg \min_{\delta \mathbf{u} \in U_h \times \Sigma_h} \|\mathcal{R}'(\mathbf{u}_n) \delta \mathbf{u} - \mathbf{f} + \mathcal{R}(\mathbf{u}_n)\|_H^2$$

if $\xi_n \leq \eta_n \|\mathcal{R}(\mathbf{u}_n)\|_H$ **then**stop **loop****end if**Compute error estimator $\eta_n(T) = \mathcal{F}_{\text{lin}}(\delta \mathbf{u}_n; \mathbf{R}(\mathbf{u}_n))$ for every $T \in \mathcal{T}$ Mark minimal set of elements \mathcal{M} such that $\sum_{T \in \mathcal{M}} \eta_n(T) \leq \theta \sum_{T \in \mathcal{T}} \eta_n(T)$ Refine all marked elements \mathcal{M} of the mesh \mathcal{T} and set the new mesh as \mathcal{T} **end loop****return** $\delta \mathbf{u}_n$

To perform the Gauss-Newton method in practice, an inexact minimization results in the residual

$$\xi_n = \|\mathcal{R}'(\mathbf{u}_n) \delta \mathbf{u}_n - \mathbf{f} + \mathcal{R}(\mathbf{u}_n)\|_H. \quad (14)$$

The convergence of the inexact Gauss-Newton, cf. Algorithm 4 is guaranteed by the introduction of the forcing sequence (9). The AFEM-loop in Algorithm 3 dynamically refines the mesh to resolve local features of the solution, ensuring optimal accuracy with minimal computational cost. For more details regarding the convergence of the AFEM-loop, please refer to [5].

This AFEM-loop, can now be integrated into the inexact Newton framework, as its adaptive refinement is essential for accurately approximating the Newton direction and optimizing computational efficiency. The resulting combined approach is detailed in Algorithm 4.

Algorithm 4 inexact Gauss-Newton

Require: initial guess \mathbf{u}_0 **Require:** $\tau \in (0, 1)$ **Require:** marking parameter $\theta \in (0, 1)$ Set $n = 0$ Set $\eta_n = \tau$ **while** stopping criterion not met **do**Determine a Newton direction $\delta \mathbf{u}_n$ by Algorithm 3Set $\mathbf{u}_{n+1} = \mathbf{u}_n + \delta \mathbf{u}_n$ Set $n = n + 1$ Set $\eta_n = \min\{\tau \eta_{n-1}, \|\mathcal{R}(\mathbf{u}_n)\|_H\}$ **end while**

Integrating AFEM-loop and forcing sequence into the inexact Newton method, the convergence properties of the resulting algorithm for solving nonlinear Least-Squares problems can be established in the following theorem.

Theorem 3.2. *Let assumptions 1 and 2 hold true and $K(u)$ be Fréchet differentiable in S . Moreover, let $(u^*, \sigma^*) \in S \times \Sigma$ denotes a solution of $\mathcal{R}(\mathbf{u}) = 0$. Then, the convergence of Algorithm 3 implies that there exists $\varepsilon > 0$ such that for any initial guess \mathbf{u}_0 in $B(\mathbf{u}^*, \varepsilon)$, it holds:*

- (a) *The inexact Newton method is well-defined and generates a sequence (\mathbf{u}_n) which converges to \mathbf{u}^* .*
- (b) *\mathbf{u}^* is the unique solution of $\mathcal{R}(\mathbf{u}) = 0$ in $B(\mathbf{u}^*, \varepsilon)$.*
- (c) *The sequence (\mathbf{u}_n) generated by Algorithm 4, converges superlinearly.*

(d) If additionally K' is Lipschitz continuous on $B(\mathbf{u}^*, \varepsilon)$, then (\mathbf{u}_n) generated by Algorithm 4 converges quadratically.

Proof. Theorem 3.1 establishes the critical norm equivalence (6), ensuring well-posedness of the Least-Squares functional. Assumption 1 and the Fréchet differentiability of $K(u)$ shows that $\mathcal{R}(\mathbf{u})$ is Fréchet differentiability for all $\mathbf{u} \in U \subset S$. With these properties in place, the conditions required to apply Theorem 2.2 are satisfied. Specifically, the inexact Newton method is well-defined and converges under the forcing sequence condition (9). \square

The results so far demonstrate that the combination of norm equivalence, adaptive refinement through the AFEM-loop, and the inexact Newton framework ensures robust convergence of the Gauss-Newton method. One can now build on these previous results to focus on the use of the Least-Squares functional in posteriori error estimation. First, the assumptions 1 and 2 are shown to imply the norm-equivalence of the nonlinear Least-Squares functional, which in turn forms the basis for deriving reliable and efficient a posteriori error estimates. It is important to note that, unlike the previous results, this analysis does not assume the Fréchet differentiability of $K(u)$, allowing the use of the error estimate for a broader class of nonlinear problems.

Theorem 3.3. *Let $(u, \sigma) \in U \times \Sigma$ solve the underlying PDE and the assumptions 1 and 2 hold true. Then the Least-Squares functional (10) is a reliable and efficient error estimator, i.e. it holds*

$$C_{\text{rel}} (\|u - v\|_U^2 + \|\sigma - \tau\|^2) \leq \mathcal{F}(v, \tau; f, g) \leq C_{\text{eff}} (\|u - v\|_U^2 + \|\sigma - \tau\|^2) \quad (15)$$

for all $(v, \tau) \in S \times \Sigma$. The constants are given by

$$\begin{aligned} C_{\text{rel}} &= \min\{C_1(1 - C) + L(1 - C^{-1}), C_2(1 - C)\} = C_c, \\ C_{\text{eff}} &= \max\{C_3 + 2(C_5 + L), C_4 + 2C_6\} = C_s. \end{aligned}$$

for any positive constant C satisfying $\frac{1}{C_1} < C < 1$.

Proof. Since (u, σ) is the solution of the minimization problem $\mathcal{F}(u, \sigma; f, g) = 0$, it holds

$$\begin{aligned} \mathcal{F}(v, \tau; f, g) &= \|L_1(v, \tau) + f\|_H^2 + \|L_2(v, \tau) + K(v) + g\|_H^2 \\ &= \|L_1(u - v, \sigma - \tau)\|_H^2 + \|L_2(u - v, \sigma - \tau) + K(u) - K(v)\|_H^2. \end{aligned}$$

On the one hand, this leads to the efficiency

$$\begin{aligned} \mathcal{F}(v, \tau; f, g) &= \|L_1(v, \tau) + f\|_H^2 + \|L_2(v, \tau) + K(v) + g\|_H^2 \\ &= \|L_1(u - v, \sigma - \tau)\|_H^2 + \|L_2(u - v, \sigma - \tau) + K(u) - K(v)\|_H^2 \\ &\leq \|L_1(u - v, \sigma - \tau)\|_H^2 + 2\|L_2(u - v, \sigma - \tau)\|_H^2 + 2\|K(u) - K(v)\|_H^2 \\ &\leq (C_3 + 2(C_5 + L))\|u - v\|_U^2 + (C_4 + 2C_6)\|\sigma - \tau\|_\Sigma^2. \end{aligned}$$

On the other hand, Young's inequality implies

$$\begin{aligned} \mathcal{F}(v, \tau; f, g) &\geq \|L_1(u - v, \sigma - \tau)\|_H^2 + (1 - C)\|L_2(u - v, \sigma - \tau)\|_H^2 - (C^{-1} - 1)\|K(u) - K(v)\|_H^2 \\ &\geq C_2(1 - C)\|\sigma - \tau\|_\Sigma^2 + (C_1(1 - C) - L(C^{-1} - 1))\|u - v\|_U^2 \end{aligned}$$

and since $(C_1(1 - C) + L(1 - 1/C)) > 0$ and $C_2(1 - C) > 0$, the reliability estimate holds true. \square

In conclusion, the Least-Squares functional can serve as an a posteriori error estimation under Assumptions 1 and 2. The reliability and efficiency of the functional were shown to hold for a wide class of nonlinear problems, even without requiring the Fréchet differentiability of $K(u)$. To further illustrate these results, practical examples will be presented in the next section.

4. Application of the framework

Up to this point, it has been proven that nonlinear Least-Squares functionals of a specific form serve as a posteriori error estimators. In the following section this theory will be applied to a nonlinear Poisson problem with Lipschitz continuous coefficient as well as a source term with ReLU-type nonlinearity, the nonlinear Saint Venant–Kirchhoff model of elasticity and a model for sea-ice dynamics. Across the various applications, different boundary conditions are handled by decomposing the boundary $\partial\Omega$ into Γ_D and Γ_N , with $\partial\Omega = \Gamma_D \cup \Gamma_N$. The following usual Sobolev spaces

$$\begin{aligned} H_0^1(\Omega) &= \{v \in H^1(\Omega) : v|_{\partial\Omega} = 0\}, \\ H_{\Gamma_D}^1(\Omega) &= \{v \in H^1(\Omega; \mathbb{R}^d) : v = 0 \text{ on } \Gamma_D\}, \\ H_{\Gamma_N}(\text{div}; \Omega) &= \{\tau \in H(\text{div}, \Omega) : \tau \cdot \nu = 0 \text{ on } \Gamma_N\} \end{aligned}$$

are used.

4.1. Stationary heat equation with temperature-dependent thermal conductivity

The simplest case study for the nonlinear Least-Squares methodology is the quasilinear stationary heat equation with temperature-dependent thermal conductivity, as discussed e.g. in [1]. This equation seeks $u \in H_{\Gamma_D}^1(\Omega)$ such that

$$-\text{div}(\kappa(u)\nabla u) = f \text{ in } \Omega, \quad u = 0 \text{ on } \Gamma_D, \quad \nabla u \cdot \nu = 0 \text{ on } \Gamma_N \quad (16)$$

with $\kappa(u)$ is Lipschitz continuous. The corresponding Least-Squares functional reads

$$\mathcal{F}_1(u, \sigma; f) = \|f - \text{div } \sigma\|^2 + \|\kappa(u)\nabla u + \sigma\|^2. \quad (17)$$

Recasting this first order system into the framework (10), requires the solution of the unconstrained minimization problem

$$\text{minimize } \mathcal{F}_1(u, \sigma; f) = \|L_1(u, \sigma) + f\|^2 + \|L_2(u, \sigma) + K(u)\|^2, \quad (18)$$

in $H_{\Gamma_D}^1(\Omega) \times H_{\Gamma_N}(\text{div}; \Omega)$ with

$$\begin{aligned} K(u) &= (1 + \kappa(u))\nabla u \\ L_1(\sigma) &= -\text{div } \sigma \\ L_2(\sigma) &= \sigma - \nabla u. \end{aligned}$$

Clearly, the functional $\|\text{div } \sigma\|^2 + \|\sigma - \nabla u\|^2$ is elliptic (see e.g. [14]). However, to provide explicit constants and ensure quantitative estimates in the following analysis, recall the following technical lemma.

Lemma 4.1. *Let $\kappa \in \mathbb{R}$ and $C_P > 0$. For any $\alpha \in \left(\max\left(0, \frac{C_P^2 - 1}{C_P^2 + 1}\right), 1\right)$ there exists $\beta, \gamma > 0$ such that*

$$1 - \frac{(1-\alpha)^2 \kappa^2}{\gamma} > 0, \quad \kappa^2 - \beta - \gamma C_P^2 > 0, \quad 1 - \frac{\alpha^2 \kappa^2}{\beta} > 0.$$

Proof. In particular, $\gamma > (1 - \alpha)^2 \kappa^2$ and $\beta > \alpha^2 \kappa^2$ implies $\kappa^2 > \beta + \gamma C_P^2 > (1 - \alpha)^2 \kappa^2 C_P^2 + \alpha^2 \kappa^2$ and this is only possible if

$$\kappa^2 > (1 - \alpha)^2 \kappa^2 C_P^2 + \alpha^2 \kappa^2$$

i.e. $g(\alpha) > 0$ with $g(\alpha) = 1 - (1 - \alpha)^2 C_P^2 - \alpha^2$. It holds

$$g(\alpha) = -\alpha^2(C_P^2 + 1) + 2\alpha C_P^2 + (1 - C_P^2) = (C_P^2 + 1)(1 - \alpha) \left(\alpha - \frac{C_P^2 - 1}{C_P^2 + 1} \right)$$

such that g admits two roots given by $\overline{\alpha} = 1$ and $\underline{\alpha} = \frac{C_P^2 - 1}{C_P^2 + 1}$ and g is positive on $[\underline{\alpha}, 1]$. Moreover, the derivative of g is given by

$$g'(\alpha) = -2\alpha(C_P^2 + 1) + 2C_P^2$$

with its maximum attained for

$$\alpha_{\max} = \frac{C_P^2}{C_P^2 + 1} \in [\underline{\alpha}, 1] \text{ with } g(\alpha_{\max}) = (C_P^2 + 1) \left(1 - \frac{C_P^2}{C_P^2 + 1} \right) \left(\frac{C_P^2}{C_P^2 + 1} - \frac{C_P^2 - 1}{C_P^2 + 1} \right) \frac{1}{C_P^2 + 1}.$$

Thus, $g : \left[\max\left(0, \frac{C_P^2 - 1}{C_P^2 + 1}\right), 1 \right] \rightarrow [0, \frac{1}{C_P^2 + 1}]$ is bijective. Moreover $\hat{\alpha} \in \left(\max\left(0, \frac{C_P^2 - 1}{C_P^2 + 1}\right), 1 \right)$ implies $g(\hat{\alpha}) > 0$, i.e.

$$\frac{1 - \hat{\alpha}^2}{C_P^2} > (1 - \hat{\alpha})^2$$

such that it is possible to choose

$$\hat{\gamma} \in \left((1 - \hat{\alpha})^2 \kappa^2, \frac{\kappa^2}{C_P^2} (1 - \hat{\alpha}^2) \right), \hat{\beta} \in \left(\hat{\alpha}^2 \kappa^2, \kappa^2 - \hat{\gamma} C_P^2 \right).$$

□

Theorem 4.2. *Let κ be constant and*

$$\mathcal{F}_{1,l}(u, \sigma; 0) = \|\operatorname{div} \sigma\|^2 + \|\kappa \nabla u + \sigma\|^2.$$

There exists a constant $\lambda > 0$ such that

$$\mathcal{F}_{1,l}(u, \sigma; 0) \geq \lambda \left(\|\operatorname{div} \sigma\|^2 + \|\nabla u\|^2 + \|\sigma\|^2 \right) \text{ for all } (u, \sigma) \in H_{\Gamma_D}^1(\Omega) \times H_{\Gamma_N}(\operatorname{div}; \Omega).$$

Proof. With a parameter $\alpha \in (0, 1)$, the functional reads

$$\mathcal{F}_{1,l}(u, \sigma; 0) = \|\operatorname{div} \sigma\|^2 + \kappa^2 \|\nabla u\|^2 + \|\sigma\|^2 - 2\alpha \kappa \langle \nabla u, \sigma \rangle - 2(1 - \alpha) \kappa \langle \nabla u, \sigma \rangle.$$

and integrating by parts leads to

$$\mathcal{F}_{1,l}(u, \sigma; 0) = \|\operatorname{div} \sigma\|^2 + \kappa^2 \|\nabla u\|^2 + \|\sigma\|^2 - 2\alpha \kappa \langle \nabla u, \sigma \rangle + 2(1 - \alpha) \kappa \langle u, \operatorname{div} \sigma \rangle.$$

For some $\beta > 0$ and $\gamma > 0$ it holds

$$-2\alpha \kappa \langle \nabla u, \sigma \rangle \geq -\left[\beta \|\nabla u\|^2 + \frac{\alpha^2 \kappa^2}{\beta} \|\sigma\|^2 \right],$$

and

$$2(1 - \alpha) \kappa \langle u, \operatorname{div} \sigma \rangle \geq -\left[\gamma \|u\|^2 + \frac{(1 - \alpha)^2 \kappa^2}{\gamma} \|\operatorname{div} \sigma\|^2 \right],$$

yields

$$\mathcal{F}_{1,l}(u, \sigma; 0) \geq \left[1 - \frac{(1 - \alpha)^2 \kappa^2}{\gamma} \right] \|\operatorname{div} \sigma\|^2 + \left[\kappa^2 - \beta \right] \|\nabla u\|^2 + \left[1 - \frac{\alpha^2 \kappa^2}{\beta} \right] \|\sigma\|^2 - \gamma \|u\|^2.$$

The Poincaré–Friedrichs inequality $\|u\| \leq C_P \|\nabla u\|$ leads to

$$\mathcal{F}_{1,l}(u, \sigma; 0) \geq \left[1 - \frac{(1 - \alpha)^2 \kappa^2}{\gamma} \right] \|\operatorname{div} \sigma\|^2 + \left[\kappa^2 - \beta - \gamma C_P^2 \right] \|\nabla u\|^2 + \left[1 - \frac{\alpha^2 \kappa^2}{\beta} \right] \|\sigma\|^2.$$

According to Lemma 4.1, $\alpha \in (0, 1)$, $\beta > 0$ and $\gamma > 0$ can be found such that

$$1 - \frac{(1 - \alpha)^2 \kappa^2}{\gamma} > 0, \quad 1 - \frac{\alpha^2 \kappa^2}{\beta} > 0, \quad \text{and} \quad 1 - \frac{\alpha^2 \kappa^2}{\beta} > 0 \quad (19)$$

holds, and set

$$\lambda = \min \left\{ 1 - \frac{(1 - \hat{\alpha})^2 \kappa^2}{\gamma}, \kappa^2 - \beta - \gamma C_P^2, 1 - \frac{\hat{\alpha}^2 \kappa^2}{\beta} \right\}.$$

□

Lemma 4.3. Assume that the system (16) admits a solution $u^* \in H_{\Gamma_D}^1(\Omega)$. Then, there exists $\varepsilon > 0$ such that $K(u)$ satisfies Assumption 2 on $B(u^*, \varepsilon)$.

Proof. Since κ is Lipschitz-continuous, $(1 - \kappa(u))\nabla u$ is differentiable and for any constant $C_1 > 0$, there exists $\varepsilon > 0$ such that

$$\|K(u) - K(v)\|^2 \leq C_1 \|u - v\|_U^2 \quad (20)$$

holds for all $u, v \in B(u^*, \varepsilon)$. \square

The previous Theorem 4.2 and Lemma 4.3 imply that the assumptions 1 and 2 hold. Consequently, Theorems 3.1 and 3.3 apply, which means that the Least-Squares functional (17) serves as an error indicator for the nonlinear, quasi-stationary heat equation. Corresponding numerical results demonstrate this for two domains, a rectangle, as well as an L-shape made of silicon with variable thermal conductivity

$$\kappa(u) = 6.27 u^4 - 13.26 u^3 + 9.98 u^2 - 5.41 u + 2.68$$

with respect to a dimensionless temperature

$$u = \frac{\theta - 200\text{K}}{800\text{K}} \quad (21)$$

based on the measurements of [11].

Example 1:

At first a unit-square with manufactured solution

$$u = \sin(\pi x) \cos(\pi y) + 0.1 (x + y)^2 + 0.4 \quad \text{and} \quad f = -\operatorname{div}(\kappa(u) \nabla u)$$

is considered. Pure Dirichlet boundary conditions are applied on the entire boundary $\partial\Omega$. The experimental order of convergence (e.o.c) of the error as well as the Least-Squares functional (18) under uniform mesh refinement are reported in Table 1. Optimal convergence ratios of the error

$$\|\mathbf{u} - \mathbf{u}_h\|^2 = \|\nabla(u - u_h)\|^2 + \|\sigma - \sigma_h\|^2 + \|\operatorname{div}(\sigma - \sigma_h)\|^2$$

as well as the Least-Squares functional are achieved for first and second order approximations. The efficiency of the error estimate is close to one, the Gauss-Newton procedure requires 5-7 iterations to converge.

h	$k = 1$					$k = 2$				
	$\ \mathbf{u} - \mathbf{u}_h\ $	$\mathcal{F}_1^{1/2}$	i_{eff}	$\ \mathbf{u} - \mathbf{u}_h\ $	$\mathcal{F}_1^{1/2}$	i_{eff}	$\ \mathbf{u} - \mathbf{u}_h\ $	$\mathcal{F}_1^{1/2}$	i_{eff}	i_{eff}
1/2	4.59e + 0	–	4.58e + 0	–	1.00	1.56e + 0	–	1.56e + 0	–	1.0
1/4	2.41e + 0	0.93	2.41e + 0	0.92	1.00	4.05e – 1	0.98	4.06e – 1	1.07	1.0
1/8	1.16e + 0	1.05	1.17e – 1	1.04	1.01	1.41e – 1	0.99	1.41e – 1	0.80	1.0
1/16	5.88e – 1	0.99	5.93e – 1	0.98	1.01	3.56e – 2	1.01	3.57e – 2	1.02	1.0
1/32	2.95e – 1	1.00	2.97e – 1	1.00	1.01	8.91e – 3	1.01	8.94e – 3	1.01	1.0
1/64	1.47e – 1	1.00	1.49e – 1	1.00	1.01	2.23e – 3	1.00	2.24e – 3	1.01	1.0

Table 1: Convergence history for a manufactured solution of the stationary heat equation with temperature dependent conductivity: Values for the error $\|\mathbf{u} - \mathbf{u}_h\|$, the Least-Squares functional \mathcal{F}_1 and the effectivity index i_{eff} using $u_h \in (\mathbf{P}_k)^2$ and $\sigma_h \in (\mathbf{RT}_{k-1})^2$ with $k \in \{1, 2\}$.

Example 2:

In order to highlight the use of the Least-Squares functional as an error estimator, the second example considers an L-shaped domain $\Omega = [-1, 1]^2 \setminus [0, 1]$ with mixed boundary conditions

$$\begin{aligned} u &= 0.00 && \text{on } \{(x, y) \in \partial\Omega : x = 1\} \\ u &= 0.85 && \text{on } \{(x, y) \in \partial\Omega : y = 1\} \\ \nabla u \cdot \nu &= 0.00 && \text{on } \{(x, y) \in \partial\Omega : x \neq 1 \wedge y \neq 1\} . \end{aligned}$$

A spatially constant source term $f = -0.05$ is applied. Due to the singularity in the reentrant corner, adaptive mesh refinement is applied, using a Dörfler marking strategy with a bulk parameter of 0.5 for first- respectively 0.8 for second order approximations. The resulting mesh after six refinement cycles as well as the dimensionless temperature field are shown in Figure 1.

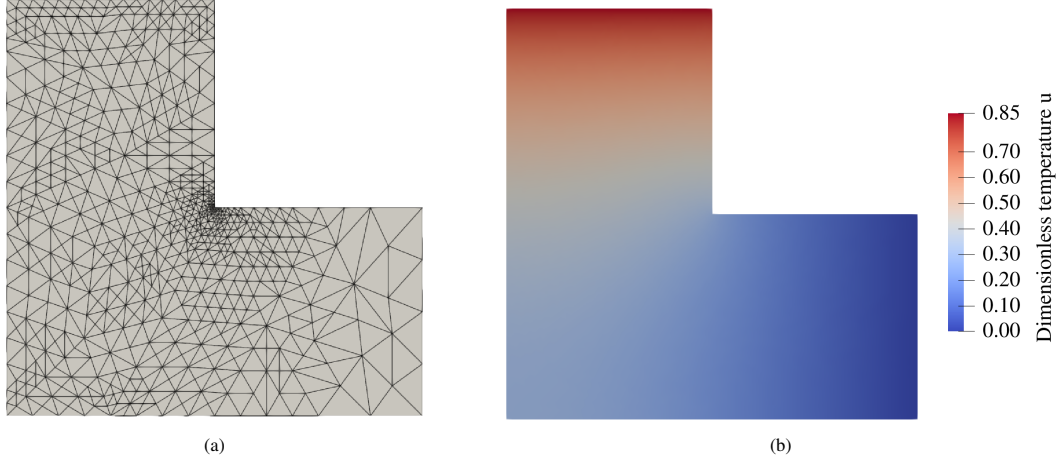


Figure 1: Solution of the stationary heat equation on an L-shaped domain using $u_h \in (P_1)^2$ and $\sigma_h \in (RT_0)^2$: The adapted mesh after six refinement cycles (a) and the corresponding solution (b).

The convergence history of two Least-Squares methods is detailed in Table 2. Optimal convergence ratios are achieved, while the effectivity indices i_{eff} of the underlying error estimators are very close to one.

k	n	n_{DOF}	$ \mathbf{u} - \mathbf{u}_h $		$\mathcal{F}_1^{1/2}$		i_{eff}
1	1	81	$2.22e-1$	–	$2.37e-1$	–	1.07
1	2	131	$1.82e-1$	0.40	$1.80e-1$	0.55	1.00
1	3	221	$1.49e-1$	0.39	$1.46e-1$	0.41	0.99
1	4	366	$1.13e-1$	0.54	$1.08e-1$	0.59	0.96
1	9	7366	$2.31e-2$	0.47	$2.00e-2$	0.51	0.99
1	10	14328	$1.62e-2$	0.54	$1.45e-2$	0.49	1.02
2	1	257	$8.72e-2$	–	$9.89e-2$	–	1.13
2	2	443	$6.23e-2$	0.62	$6.52e-2$	0.77	1.05
2	3	643	$4.92e-2$	0.63	$4.53e-2$	0.98	0.92
2	4	1028	$2.47e-2$	1.47	$2.65e-2$	1.14	1.08
2	9	9022	$2.64e-3$	0.96	$2.96e-3$	0.97	1.12
2	10	14913	$1.69e-3$	0.89	$1.86e-3$	0.92	1.10

Table 2: Convergence history of the stationary heat equation with temperature dependent conductivity on an L-shaped domain: Values for the error $|||\mathbf{u} - \mathbf{u}_h|||$, the Least-Squares functional \mathcal{F}_1 and the effectivity index i_{eff} using $u_h \in (P_k)^2$ and $\sigma_h \in (RT_{k-1})^2$ with $k \in \{1, 2\}$.

4.2. Remarks on discontinuous coefficients

For completeness, note that extending the analysis to the case of discontinuous coefficients poses no additional difficulties. To this end, let Ω be partitioned into two subdomains Ω_1 and Ω_2 , on each of which the parameter is constant

$$\kappa(x) = \begin{cases} \kappa_1, & x \in \Omega_1 \\ \kappa_2, & x \in \Omega_2 \end{cases}.$$

Then, on each subdomain Ω_i , integrating by parts yields

$$\begin{aligned} \mathcal{F}_{1,i}(u, \sigma; 0) \Big|_{\Omega_i} &= \|\operatorname{div} \sigma\|_{L^2(\Omega_i)}^2 + \kappa_i^2 \|\nabla u\|_{L^2(\Omega_i)}^2 + \|\sigma\|_{L^2(\Omega_i)}^2 \\ &\quad - 2\alpha \kappa_i \langle \nabla u, \sigma \rangle_{\Omega_i} + 2(1-\alpha) \kappa_i \langle u, \operatorname{div} \sigma \rangle_{\Omega_i} - 2(1-\alpha) \kappa_i \int_{\partial\Omega_i} u (\sigma \cdot n) ds. \end{aligned}$$

Since $u = 0$ on the external boundary, the only non-vanishing boundary contributions arise from the internal interface $\Gamma = \partial\Omega_1 \cap \partial\Omega_2$ and the interface term can be estimated using the duality between $H^{1/2}(\Gamma)$ and $H^{-1/2}(\Gamma)$. Indeed

$$\langle u, \sigma \cdot n \rangle_{\Gamma} \leq \|u\|_{H^{1/2}(\Gamma)} \|\sigma \cdot n\|_{H^{-1/2}(\Gamma)},$$

and the Young's inequality with parameter $\delta > 0$ yields

$$-2(1-\alpha)(\kappa_1 - \kappa_2) \langle u, \sigma \cdot n \rangle_{\Gamma} \geq -\delta \|u\|_{H^{1/2}(\Gamma)}^2 - \frac{(1-\alpha)^2(\kappa_1 - \kappa_2)^2}{\delta} \|\sigma \cdot n\|_{H^{-1/2}(\Gamma)}^2.$$

Moreover, combining the standard trace inequality with the Poincaré–Friedrichs inequality leads to

$$\begin{aligned} \|u\|_{H^{1/2}(\Gamma)}^2 &\leq C_{tr,u}^2 (\|u\|_{L^2(\Omega)}^2 + \|\nabla u\|_{L^2(\Omega)}^2) \leq C_{tr,u}^2 (1 + C_P^2) \|\nabla u\|_{L^2(\Omega)}^2, \\ \text{and } \|\sigma \cdot n\|_{H^{-1/2}(\Gamma)}^2 &\leq C_{tr,\sigma}^2 (\|\sigma\|_{L^2(\Omega)}^2 + \|\operatorname{div} \sigma\|_{L^2(\Omega)}^2). \end{aligned}$$

Thus, the coercivity estimate reads

$$\begin{aligned} \mathcal{F}_{1,i}(u, \sigma; 0) &\geq \sum_{i=1}^2 \left\{ \left[\left(1 - \frac{(1-\alpha)^2 \kappa_i^2}{\gamma_i} \right) - \frac{(1-\alpha)^2(\kappa_1 - \kappa_2)^2}{\delta} C_{tr,\sigma}^2 \right] \|\operatorname{div} \sigma\|_{L^2(\Omega_i)}^2 \right. \\ &\quad + \left[\left(1 - \frac{\alpha^2 \kappa_i^2}{\beta_i} \right) - \frac{(1-\alpha)^2(\kappa_1 - \kappa_2)^2}{\delta} C_{tr,\sigma}^2 \right] \|\sigma\|_{L^2(\Omega_i)}^2 \\ &\quad \left. + [\kappa_i^2 - \beta_i - \gamma_i C_P^2 - \delta C_{tr,u}^2 (1 + C_P^2)] \|\nabla u\|_{L^2(\Omega_i)}^2 \right\}. \end{aligned}$$

In a first step, choose

$$\delta = \theta \frac{\min_{i=1,2} \{\kappa_i^2 - \beta_i - \gamma_i C_P^2\}}{C_{tr,u}^2 (1 + C_P^2)}.$$

According to Lemma 4.1 $1 - \alpha$ can now be chosen small enough to ensure that all the terms remains positive.

4.3. ReLU Activation

Equations involving ReLU-type nonlinearities appear frequently in control theory and physics-informed machine learning. A representative example is

$$-\Delta u + \max(u, 0) = f \quad \text{in } \Omega.$$

To cast this second-order PDE into the presented framework, a flux variable $\sigma = \nabla u$ is introduced. Then the PDE is reformulated as first-order system

$$\sigma - \nabla u = 0, \quad \operatorname{div} \sigma + \max(u, 0) = f. \quad (22)$$

Note that setting

$$\begin{aligned} L_1(u, \sigma) &:= \sigma - \nabla u, \\ L_2(u, \sigma) &:= -\operatorname{div} \sigma, \\ K(u) &:= \max(u, 0). \end{aligned}$$

with the corresponding Least-Squares functional

$$\|\sigma - \nabla u\| + \|\sigma - \operatorname{div} \sigma + \max(u, 0)\|.$$

would not satisfy assumptions 2. In fact, the nonlinear term $K(u) = \max(u, 0)$ is Lipschitz continuous with Lipschitz constant $L = 1$ while in the analysis of the previous examples, one obtains $\|L_1(u, \sigma)\| + \|L_2(u, \sigma)\| \geq C_1 \|u\|_1^2 + C_2 \|\sigma\|_{div}^2$ with $C_1 < 1$. $K(u)$ therefore needs to be shifted. To this end, note that the function $\max(u, 0) - \delta u$ for some $\delta > 0$ is Lipschitz continuous with Lipschitz constant $\max(|1 - \delta|, |\delta|)$. Weighting the first term with κ and choosing $\delta > 1$ it remains to prove

$$\mathcal{F}_2(u, \sigma; 0) = \|L_1(u, \sigma)\| + \|L_2(u, \sigma)\| \geq C_1 \|u\|_1^2 + C_2 \|\sigma\|_{div}^2$$

with $C_1 > \delta$ for

$$L_1(u, \sigma) := \kappa(\sigma - \nabla u), \quad L_2(u, \sigma) := -\operatorname{div} \sigma + \delta u \quad K(u) := \max(u, 0) - \delta u.$$

The corresponding linear Least-Squares functional reads

$$\mathcal{F}_{2,l}(u, \sigma; f) = \|\kappa(\sigma - \nabla u)\|^2 + \|\delta u - \operatorname{div} \sigma - f\|^2$$

and integration by parts leads to

$$\begin{aligned} \mathcal{F}_{2,l}(u, \sigma; 0) &= \|L_1(u, \sigma)\|^2 + \|L_2(u, \sigma)\|^2 = \kappa^2 \|\sigma\|^2 + \kappa^2 \|\nabla u\|^2 + \|\operatorname{div} \sigma\|^2 + \delta^2 \|u\|^2 - 2(\kappa^2 - \delta) \langle \sigma, \nabla u \rangle \\ &\geq \left[\kappa^2 - \varepsilon(\kappa^2 - \delta) \right] \|\sigma\|^2 + \left[\kappa^2 - \frac{\kappa^2 - \delta}{\varepsilon} \right] \|\nabla u\|^2 + \|\operatorname{div} \sigma\|^2 + \delta^2 \|u\|^2. \end{aligned}$$

For $1 < \delta < \kappa^2$, ε can be chosen to satisfy

$$1 < \varepsilon < \frac{\kappa^2}{\kappa^2 - \delta}.$$

and it holds

$$\kappa^2 - \frac{\kappa^2 - \delta}{\varepsilon} > \kappa^2 - (\kappa^2 - \delta) = \delta.$$

Since $\delta > 1$, $\delta^2 > \delta$ this leads to

$$\mathcal{F}_{2,l}(u, \sigma; 0) > C_2 \|\sigma\|_{div}^2 + \delta \|u\|_1^2$$

with $C_2 > 0$. Consequently, the assumptions 1 and 2 hold true and the theorems 3.1 and 3.3 apply. The Least-Squares functional $\mathcal{F}_{2,l}$ can be used as an error indicator, as in the following numerical example based on the previously used L-shape $\Omega = [-1, 1]^2 \setminus [0, 1]$. With the modified, mixed boundary conditions

$$\begin{aligned} u &= -2.0 && \text{on } \{(x, y) \in \partial\Omega : x = 1\} \\ u &= 3.0 && \text{on } \{(x, y) \in \partial\Omega : y = 1\} \\ \nabla u \cdot \nu &= 0.0 && \text{on } \{(x, y) \in \partial\Omega : x \neq 1 \wedge y \neq 1\}, \end{aligned}$$

the resulting convergence history for first- and second order approximations with adaptive mesh refinement using a Dörfler marking strategy with a bulk parameter of 0.5 is given in Table 3. As predicted, optimal convergence rates are achieved. The efficiency of the error estimate is nearly equal one.

4.4. Nonlinear elasticity

A fundamental component in structural analysis is the use of displacement-based finite element formulations, which form the basis of many mechanical simulations in engineering practice. In most scenarios, materials are modeled either using elastic or elastoplastic constitutive laws, with a significant portion of applications assuming elastic behavior under small deformations or, more generally, large deformations at small strains. While elasticity for small

k	n	n_{DOF}	$ \mathbf{u} - \mathbf{u}_h $		$\mathcal{F}_2^{1/2}$		i_{eff}
1	1	81	$8.79e-1$	–	$8.71e-1$	–	0.99
1	2	131	$6.64e-1$	0.58	$6.62e-1$	0.59	1.00
1	3	232	$5.16e-1$	0.44	$5.15e-1$	0.46	1.00
1	4	388	$3.84e-1$	0.57	$3.84e-1$	0.54	1.00
1	9	8389	$7.85e-2$	0.51	$7.85e-2$	0.52	1.00
1	10	15566	$5.75e-2$	0.50	$5.75e-2$	0.50	1.00
2	1	257	$3.53e-1$	–	$3.53e-1$	–	1.00
2	2	387	$2.25e-1$	1.10	$2.24e-1$	1.10	1.00
2	3	531	$1.46e-1$	1.37	$1.46e-1$	1.36	1.00
2	4	754	$9.79e-2$	1.14	$9.78e-2$	1.14	1.00
2	9	2930	$1.93e-2$	1.10	$1.93e-2$	1.11	1.00
2	10	4279	$1.25e-2$	1.16	$1.25e-2$	1.15	1.00

Table 3: Convergence history of the stationary heat equation with ReLU-type nonlinearity on an L-shaped domain: Values for the error $|||\mathbf{u} - \mathbf{u}_h|||$, the Least-Squares functional \mathcal{F}_1 and the effectivity index i_{eff} using $u_h \in (\mathbf{P}_k)^2$ and $\sigma_h \in (\mathbf{RT}_{k-1})^2$ with $k \in \{1, 2\}$.

deformations leads to linear systems of equations, transition to the large deformation settings introduces nonlinearities. This section focuses on large deformations at small strains, for which the Saint Venant–Kirchhoff model provides a prototypical formulation. Based on deformation gradient and Green-Lagrange strain

$$\mathbf{F}(u) = \mathbf{I} + \nabla u \quad \text{respectively} \quad \mathbf{E}(u) = \frac{1}{2} \left(\mathbf{F}^T(u) \mathbf{F}(u) - \mathbf{I} \right), \quad (23)$$

the first Piola-Kirchhoff stress reads

$$\sigma(u) = \mathbf{F}(u) \left(2 \mathbf{E}(u) + \tilde{\lambda} \operatorname{tr} \mathbf{E}(u) \mathbf{I} \right) = 2 \varepsilon(u) + \tilde{\lambda} \operatorname{tr} \varepsilon(u) \mathbf{I} + k(u), \quad (24)$$

with the nonlinearity

$$k(u) = \left[2 \nabla^T u + \nabla u + \nabla u \nabla^T u + \tilde{\lambda} \operatorname{tr} \mathbf{E}(u) \right] \nabla u + \frac{\tilde{\lambda}}{2} \operatorname{tr} \left(\nabla^T u \nabla u \right) \mathbf{I}.$$

The parameter $\tilde{\lambda}$ is thereby the ratio of the first- and the second Lamé parameter. Note that the classical notation from elasticity theory \mathbf{P} (see e.g. [10]) is not used here to highlight conformance with the presented framework. Based on the compliance of linear elasticity

$$\mathcal{A}\tau = \frac{1}{2} \left[\tau - \frac{\tilde{\lambda}}{2 + d\tilde{\lambda}} \operatorname{tr} \tau \mathbf{I} \right], \quad (25)$$

and the conservation of linear momentum, weighted with a parameter $\kappa > 0$, the Least-Squares functional of the considered problem reads

$$\mathcal{F}_3(u, \sigma; f) = \kappa^2 \|\operatorname{div} \sigma + f\|^2 + \|\mathcal{A}\sigma - \varepsilon(u) - \mathcal{A}k(u)\|^2. \quad (26)$$

Within the notation of the presented framework, the unconstrained minimization problem

$$\text{minimize } \mathcal{F}_3(u, \sigma; f) = \|L_1(\sigma) + f\|^2 + \|L_2(u, \sigma) + K(u)\|^2 \quad (27)$$

in $(H_{\Gamma_D}^1(\Omega))^d \times (H_{\Gamma_N}(\operatorname{div}; \Omega))^d$, with

$$\begin{aligned} K(u) &= \mathcal{A}k(u) \\ L_1(\sigma) &= \kappa \operatorname{div} \sigma \\ L_2(\sigma) &= \mathcal{A}\sigma - \varepsilon(u) \end{aligned}$$

has to be solved.

As $K(u)$ is differentiable and the linear part of the Least-Squares functional elliptic, as is proven in the following theorem, the framework applies without further difficulties.

Theorem 4.4. *There exists a constant $C > 0$ such that for*

$$\mathcal{F}_{3,l}(u, \sigma; 0) = \|L_1(\sigma)\|^2 + \|L_2(u, \sigma)\|^2 = \|\operatorname{div} \sigma\|^2 + \|\mathcal{A}\sigma - \epsilon(u)\|^2$$

it holds $\mathcal{F}_{3,l}(u, \sigma; 0) \simeq C \left(\|\sigma\|_{div}^2 + \|u\|_1^2 \right)$

Proof. The proof makes use of the equivalence

$$\|\sigma\| \simeq \left(\sqrt{(\mathcal{A}\sigma, \sigma)} + \|\operatorname{div} \sigma\| \right). \quad (28)$$

In fact, decomposing $\|\sigma\|^2 = \|\operatorname{dev} \sigma\|^2 + \frac{1}{d} \|\operatorname{tr} \sigma\|^2$ leads to

$$(\mathcal{A}\sigma, \sigma) = \frac{1}{2} \|\operatorname{dev} \sigma\|^2 + \frac{1}{d(2 + d\lambda)} \|\operatorname{tr} \sigma\|^2$$

and invoking the trace inequality

$$\|\operatorname{tr} \sigma\| \leq C_{tr} \left(\sqrt{(\mathcal{A}\sigma, \sigma)} + \|\nabla \cdot \sigma\| \right)$$

yields

$$\|\sigma\|^2 \leq 2 (\mathcal{A}\sigma, \sigma) + \frac{C_{tr}^2}{d} \left[(\mathcal{A}\sigma, \sigma) + \|\nabla \cdot \sigma\|^2 \right].$$

The Korn inequality allows to bound the cross term as follows

$$\begin{aligned} |(\sigma, \epsilon(u))| &= |(\sigma, \nabla u) - \left(\frac{\sigma - \sigma^T}{2}, \nabla u \right)| \leq |(\operatorname{div} \sigma, u)| + \left| \left(\frac{\sigma - \sigma^T}{2}, \nabla u \right) \right| \\ &\leq \|\operatorname{div} \sigma\| \|u\| + \left\| \frac{\sigma - \sigma^T}{2} \right\| \|\nabla u\| \leq C_K \left(\|\operatorname{div} \sigma\| + \left\| \frac{\sigma - \sigma^T}{2} \right\| \right) \|\epsilon(u)\|. \end{aligned}$$

Moreover,

$$\|\sigma - \sigma^T\| = 2\mu \left\| \left(\frac{1}{2\mu} \sigma - \epsilon(u) \right) - \left(\frac{1}{2\mu} \sigma - \epsilon(u) \right)^T \right\| = 2\mu \|(\mathcal{A}\sigma - \epsilon(u)) - (\mathcal{A}\sigma - \epsilon(u))^T\| \leq 4\mu \|\mathcal{A}\sigma - \epsilon(u)\|$$

leads to

$$|(\sigma, \epsilon(u))| \leq C_K \left(\|\operatorname{div} \sigma\| + \|\mathcal{A}\sigma - \epsilon(u)\| \right) \|\epsilon(u)\|.$$

Since $\mathcal{A}\sigma$ is bounded by σ in the L^2 norm, one can insert

$$\|\epsilon(u)\| \leq \|\epsilon(u) - \mathcal{A}\sigma\| + \|\mathcal{A}\sigma\| \leq \|\epsilon(u) - \mathcal{A}\sigma\| + \frac{1}{2\mu} \|\sigma\|$$

to obtain

$$|(\sigma, \epsilon(u))| \leq C_K \left(\|\operatorname{div} \sigma\| + \|\mathcal{A}\sigma - \epsilon(u)\| \right) \left(\|\epsilon(u) - \mathcal{A}\sigma\| + \frac{1}{2\mu} \|\sigma\| \right).$$

Therefore,

$$|(\sigma, \epsilon(u))| \leq C_K \sqrt{F_{3,l}(u, \sigma; 0)} \left(\sqrt{F_{3,l}(u, \sigma; 0)} + \|\sigma\| \right) = C_K \left(F_{3,l}(u, \sigma; 0) + \sqrt{F_{3,l}(u, \sigma; 0)} \|\sigma\| \right)$$

implies

$$\begin{aligned} (\mathcal{A}\sigma, \sigma) &= (\mathcal{A}\sigma - \epsilon(u), \sigma) + (\epsilon(u), \sigma) \leq \|\mathcal{A}\sigma - \epsilon(u)\| \|\sigma\| + C_K \left(F_{3,l}(u, \sigma; 0) + \sqrt{F_{3,l}(u, \sigma; 0)} \|\sigma\| \right) \\ &\leq C_K F_{3,l}(u, \sigma; 0) + \left(\|\mathcal{A}\sigma - \epsilon(u)\| + C_K \sqrt{F_{3,l}(u, \sigma; 0)} \right) \|\sigma\|. \end{aligned}$$

The norm equivalence (28)

$$\|\sigma\| \leq \tilde{C}_{tr} \left(\sqrt{(\mathcal{A}\sigma, \sigma)} + \|\operatorname{div} \sigma\| \right)$$

and $\|\operatorname{div} \sigma\|^2 \leq F_{3,l}(u, \sigma; 0)$ yields

$$\|\sigma\| \leq \tilde{C}_{tr} \left(\sqrt{(\mathcal{A}\sigma, \sigma)} + \sqrt{F_{3,l}(u, \sigma; 0)} \right).$$

Thus,

$$\begin{aligned} \|\mathcal{A}\sigma - \varepsilon(u)\| \|\sigma\| &\leq \|\mathcal{A}\sigma - \varepsilon(u)\| \tilde{C}_{tr} \left(\sqrt{(\mathcal{A}\sigma, \sigma)} + \sqrt{F_{3,l}(u, \sigma; 0)} \right) \\ &\leq \tilde{C}_{tr} \sqrt{F_{3,l}(u, \sigma; 0)} \sqrt{(\mathcal{A}\sigma, \sigma)} + \tilde{C}_{tr} F_{3,l}(u, \sigma; 0). \end{aligned}$$

and

$$\begin{aligned} C_K \sqrt{F_{3,l}(u, \sigma; 0)} \|\sigma\| &\leq C_K \sqrt{F_{3,l}(u, \sigma; 0)} \tilde{C}_{tr} \left(\sqrt{(\mathcal{A}\sigma, \sigma)} + \sqrt{F_{3,l}(u, \sigma; 0)} \right) \\ &= C_K \tilde{C}_{tr} \sqrt{F_{3,l}(u, \sigma; 0)} \sqrt{(\mathcal{A}\sigma, \sigma)} + C_K \tilde{C}_{tr} F_{3,l}(u, \sigma; 0). \end{aligned}$$

implies

$$\begin{aligned} (\mathcal{A}\sigma, \sigma) &\leq \left[\tilde{C}_{tr} \sqrt{F_{3,l}(u, \sigma; 0)} \sqrt{(\mathcal{A}\sigma, \sigma)} + \tilde{C}_{tr} F_{3,l}(u, \sigma; 0) \right] + \left[C_K \tilde{C}_{tr} \sqrt{F_{3,l}(u, \sigma; 0)} \sqrt{(\mathcal{A}\sigma, \sigma)} + C_K \tilde{C}_{tr} F_{3,l}(u, \sigma; 0) \right] \\ &= \tilde{C}_{tr}(1 + C_K) F_{3,l}(u, \sigma; 0) + \tilde{C}_{tr}(1 + C_K) \sqrt{F_{3,l}(u, \sigma; 0)} \sqrt{(\mathcal{A}\sigma, \sigma)}. \end{aligned}$$

Young's inequality yields

$$(\mathcal{A}\sigma, \sigma) \leq \tilde{C}_{tr}(1 + C_K) F_{3,l}(u, \sigma; 0) + \frac{1}{2}(\mathcal{A}\sigma, \sigma) + \frac{\tilde{C}_{tr}^2(1 + C_K)^2}{2} F_{3,l}(u, \sigma; 0)$$

i.e.

$$(\mathcal{A}\sigma, \sigma) \leq \left(2\tilde{C}_{tr}(1 + C_K) + \tilde{C}_{tr}^2(1 + C_K)^2 \right) F_{3,l}(u, \sigma; 0).$$

□

Theorems 3.1 and 3.3 thus apply, which means that the Least-Squares functional (17) serves as an error indicator. In two numerical examples, a squared domain under uniform-, and the well-known Cooks membrane (see e.g. [15]) under adaptive mesh refinement are considered.

Example 1:

A unit-square with manufactured solution

$$u = \frac{1}{10} \begin{pmatrix} \sin(\pi x) \cos(\pi y) + x^2/2\tilde{\lambda} \\ -\cos(\pi x) \sin(\pi y) + y^2/2\tilde{\lambda} \end{pmatrix} \quad \text{using} \quad f = -\operatorname{div} \sigma(u)$$

is considered. Pure Dirichlet boundary conditions are applied on the entire boundary $\partial\Omega$. The convergence history on a sequence of uniformly refined meshes is reported in Table 4. Optimal convergence ratios of the error as well as the Least-Squares functional are achieved. The efficiency of the error estimate is close to one, the Gauss-Newton procedure requires between 6 and 10 iterations to converge.

h	$ \mathbf{u} - \mathbf{u}_h $		$\mathcal{F}_3^{1/2}$		i_{eff}
1/2	$4.52e-1$	–	$4.73e-1$	–	1.05
1/4	$1.83e-1$	0.72	$1.84e-1$	0.92	1.01
1/8	$3.86e-2$	1.18	$3.88e-2$	1.04	1.01
1/16	$9.81e-3$	1.01	$9.83e-3$	0.98	1.00
1/32	$2.46e-3$	1.01	$2.46e-3$	1.00	1.00
1/64	$6.16e-4$	1.01	$6.16e-4$	1.00	1.00

Table 4: Convergence history for a manufactured solution of nonlinear elasticity: Values for the error $|||\mathbf{u} - \mathbf{u}_h|||$, the Least-Squares functional \mathcal{F}_3 and the effectivity index i_{eff} using $u_h \in (P_2)^2$, $\sigma_h \in (RT_1)^2$ and $\kappa = 1$.

Example 2:

In order to demonstrate the usage of the Least-Squares functional as marking criterion for adaptive solution procedures, the Cooks membrane is considered. The geometry with initial discretization is shown in Figure 2 (a). Within this example, displacements are approximated using quadratic Lagrangian elements $u_h \in (P_2)^2$ while the stress tensor is approximated based on a first-order Raviart-Thomas space $\sigma_h \in (RT_1)^2$. To improve convergence, a scaling factor $\kappa^2 = 10^3$ is considered. Meshes are refined using a Dörfler marking strategy with bulk parameter 0.5, leading to a considerable clustering of elements in the upper left and right as well as the lower right corners of the domain, as depicted in Figure 2 (b).

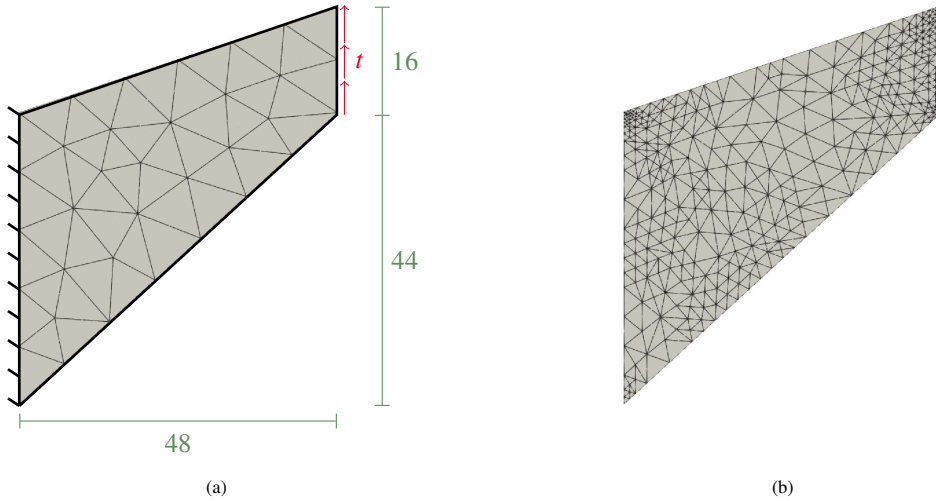


Figure 2: Cooks membrane: The boundary value problem with initial mesh (a) and the mesh after eight adaptive refinement cycles (b).

The convergence history of this experiment is detailed in Table 5. Errors are calculated based on a overkill solution on a refined grid using $u_h \in (P_3)^2$ and $\sigma_h \in (RT_2)^2$. As expected, an optimal e.o.c is achieved, while between six and eight iterations of the Gauss-Newton solver are required.

4.5. Sea-Ice

The final example examines a model of sea-ice dynamics governed by the momentum balance [3, 8]:

$$\rho h u_t = \nabla \cdot \sigma - \tau_o(u - v_o) + F(u). \quad (29)$$

Therein, u is the velocity of the sea-ice, σ the stress tensor, v_o the water velocity, $F(u)$ the external forces and $\tau_o(u)$ the ocean current, involving the water drag coefficient C_o , and the sea-water density ρ_o as well as the velocity u :

$$\tau_o(u) = \rho_o C_o |u| u.$$

n	n_{DOF}	$\ \mathbf{u} - \mathbf{u}_h\ $		$\mathcal{F}_3^{1/2}$		i_{eff}
1	754	$5.09e-1$	–	$1.31e-1$	–	0.26
2	948	$4.06e-1$	1.00	$1.03e-1$	1.03	0.26
3	1188	$3.05e-2$	1.26	$8.58e-2$	0.83	0.28
4	1614	$1.65e-2$	2.01	$6.16e-2$	1.08	0.37
7	6870	$2.85e-2$	0.96	$1.59e-2$	0.96	0.56
8	11352	$1.58e-2$	1.17	$9.74e-3$	0.97	0.62

Table 5: Convergence history for the Cooks membrane: Values for the error $\|\mathbf{u} - \mathbf{u}_h\|$, the Least-Squares functional \mathcal{F}_3 and the effectivity index i_{eff} .

With an appropriate scaling and the introduction of a parameter η , the Least-Squares functional is given by

$$\mathcal{F}_4(u, \sigma; v_o) := \|\beta^{-1/2}u + \tau_o(u) - \operatorname{div} \sigma\|^2 + \|(2\eta)^{-1/2}\sigma - (2\eta)^{1/2}\varepsilon(u) + (2\eta)^{1/2}\varepsilon(v_o)\|^2 \quad (30)$$

for given parameters $\beta, \eta > 0$. Since τ_o is differentiable the analysis reduces to the coercivity of the linear functional

$$\mathcal{F}_{4,l}(u, \sigma; 0) := \|\beta^{-1/2}u - \operatorname{div} \sigma\|^2 + \|(2\eta)^{-1/2}\sigma - (2\eta)^{1/2}\varepsilon(u)\|^2 \quad (31)$$

in $(H_{\Gamma_D}^1(\Omega))^d \times (H_{\Gamma_N}(\operatorname{div}; \Omega))^d$, shown in [6]. We refer to [3] for numerical examples on this problem.

References

- [1] G. Aguirre-Ramirez and J. T. Oden. Finite element technique applied to heat conduction in solids with temperature dependent thermal conductivity. *International Journal for Numerical Methods in Engineering*, 7(3):345–355, 1973.
- [2] Fleurianne Bertrand and Daniele Boffi. On the necessity of the inf-sup condition for a mixed finite element formulation. *IMA Journal of Numerical Analysis*, 45(1):1–35, 02 2024.
- [3] Fleurianne Bertrand and Henrik Schneider. Least-squares finite element method for the simulation of sea-ice motion. *Computers & Mathematics with Applications*, 172:38–46, 2024.
- [4] Pavel B. Bochev and Max D. Gunzburger. *Least-squares finite element methods*, volume 166 of *Applied Mathematical Sciences*. Springer, New York, 2009.
- [5] P. Bringmann and C. Carstensen. An adaptive least-squares FEM for the Stokes equations with optimal convergence rates. *Numer. Math.*, 135(2):459–492, 2017.
- [6] Zhiqiang Cai and Gerhard Starke. Least-squares methods for linear elasticity. *SIAM Journal on Numerical Analysis*, 42(2):826–842, 2005.
- [7] Peter Deufhard. *Newton methods for nonlinear problems*, volume 35 of *Springer Series in Computational Mathematics*. Springer, Heidelberg, 2011. Affine invariance and adaptive algorithms, First softcover printing of the 2006 corrected printing.
- [8] W. D. Hibler. A dynamic thermodynamic sea ice model. *Journal of Physical Oceanography*, 9(4):815–846, jul 1979.
- [9] T. A. Manteuffel, S. F. McCormick, J. G. Schmidt, and C. R. Westphal. First-order system least squares for geometrically nonlinear elasticity. *SIAM J. Numer. Anal.*, 44(5):2057–2081, 2006.
- [10] Jerrold Marsden and Thomas J. R. Hughes. *Mathematical foundations of elasticity*. Dover Publications, Inc., 1983.
- [11] Alex Masolin, Pierre-Olivier Bouchard, Roberto Martini, and Marc Bernacki. Thermo-mechanical and fracture properties in single-crystal silicon. *Journal of Materials Science*, 48(3):979–988, 2013.
- [12] Benjamin Müller, Gerhard Starke, Alexander Schwarz, and Jörg Schröder. A first-order system least squares method for hyperelasticity. *SIAM Journal on Scientific Computing*, 36(5):B795–B816, 2014.
- [13] Steffen Münenmaier. First-order system least squares for generalized-newtonian coupled stokes-darcy flow. *Numerical Methods for Partial Differential Equations*, 31(4):1150–1173, 2015.
- [14] A. I. Pehlivanov and G. F. Carey. Error estimates for least-squares mixed finite elements. *ESAIM: Modélisation mathématique et analyse numérique*, 28(5):499–516, 1994.
- [15] Jörg Schröder, Thomas Wick, Stefanie Reese, Peter Wriggers, Ralf Müller, Stefan Kollmannsberger, Markus Kästner, Alexander Schwarz, Maximilian Igelbüscher, Nils Viebahn, Hamid Reza Bayat, Stephan Wulfinghoff, Katrin Mang, Ernst Rank, Tino Bog, Davide D’Angella, Mohamed Elhaddad, Paul Hennig, Alexander Düster, Wadhah Garhuom, Simeon Hubrich, Mirjam Walloth, Winnifried Wollner, Charlotte Kuhn, and Timo Heister. A selection of benchmark problems in solid mechanics and applied mathematics. *Archives of Computational Methods in Engineering*, 28(2):713–751, March 2021.
- [16] Alexander Schwarz, Karl Steeger, Maximilian Igelbüscher, and Jörg Schröder. Different approaches for mixed ls-fems in hyperelasticity: Application of logarithmic deformation measures. *International Journal for Numerical Methods in Engineering*, 115(9):1138–1153, 2018.
- [17] G. Starke. Gauss-Newton multilevel methods for least-squares finite element computations of variably saturated subsurface flow. volume 64, pages 323–338. 2000. International GAMM-Workshop on Multigrid Methods (Bonn, 1998).
- [18] Gerhard Starke, Alexander Schwarz, and Jörg Schröder. Analysis of a modified first-order system least squares method for linear elasticity with improved momentum balance. *SIAM Journal on Numerical Analysis*, 49(3):1006–1022, 2011.
- [19] Eberhard Zeidler. *Nonlinear functional analysis and its applications. I*. Springer-Verlag, New York, 1986. Fixed-point theorems, Translated from the German by Peter R. Wadsack.